(Received 21 May 2026, Accepted 9 July 2026, Scheduled 7 August 2026)

Design of Broadband Gradient-Radius Magnetic Induction Antennas

Mingxuan Hu and Lihua Li*

Naval University of Engineering, Wuhan, Hubei 430033, China

ABSTRACT: To address the challenge of limited bandwidth in magnetic induction communication, this study proposes a magnetic induction antenna adopting a gradient-radius structure. The antenna adopts a discretized gradient-radius design, which effectively broadens the system bandwidth by increasing the antenna's resistance-to-inductance ratio. The study integrates theoretical analysis, simulation, and experimental testing to systematically investigate the effects of different taper ratio structures on resistance, inductance, and bandwidth. Experimental results demonstrated that the gradient-radius structure can significantly extend the bandwidth, and the extension effect became stronger as the taper ratio increased. Meanwhile, combined with simulation and experimental data, the attenuation effect of this structure on the near-zone magnetic field was evaluated, verifying that the bandwidth improvement came at the cost of coupling strength. Specifically, when the bandwidth was extended to nearly twice its original value, the received signal strength decreased by approximately 6.4 dBm. This study provides a simple and practical implementation approach for the broadband design of magnetic induction communication systems.

1. INTRODUCTION

Magnetic induction (MI) communication, a near-field wireless technology, is uniquely valuable in challenging environments such as underground mines and underwater detection. This is due to its minimal susceptibility to interference and high channel stability [1–3]. Compared to conventional electromagnetic-wave communication, MI communication provides a cost-effective means to enable reliable links in harsh environments, serving as a viable solution for cross-domain communication between sea-air and ground-air domains.

However, a major bottleneck of MI communication is its limited bandwidth (BW). This limitation stems from the inherently narrow bandwidth of MI antennas, which typically operate as high-quality factor resonators [4–6]. Furthermore, increasing the operating frequency leads to more severe attenuation of magnetic field signals, thereby decreasing coupling strength.

To extend the bandwidth of MI communication, existing research predominantly employed frequency-splitting techniques to generate multiple usable resonant points. For instance, Cannon utilized the strong magnetic coupling of coils to split the single-peak transmission response into a double-peak one [7]. Doan Thanh established a circuit matrix system to analyze the quantitative relationship between multi-coil structures and split frequency points [8]. Dionigi and Mongiardo introduced a parallel resonant branch into a series resonant circuit, resulting in an impedance expression containing a quartic term in the frequency, thereby generating two resonant points [9]. Agbinya and Nguyen established parallel data channels at multiple resonant frequencies to increase channel capacity [10]. However, this method introduces additional parallel resonant points between the two series resonant points, leading to a discontinuity in the available frequency band. Oh et al. partially overlapped two loop antennas with slightly different resonant frequencies and precisely adjusted the spacing to achieve zero mutual inductance, enabling the fusion of two narrow bands to expand the overall bandwidth [11]. However, this approach exhibits extreme sensitivity to coil spacing tolerance and increases the volume of the transmitting antenna. Additionally, Sun et al. utilized a series of passive relay coils with minute resonant frequency deviations to construct a frequency-shifted waveguide system, sacrificing some coupling efficiency for bandwidth extension [12]. Syms et al. employed a special fabrication process to design adjacent coils in a waveguide system with an overlapping structure, thereby broadening the passband based on the dispersion relation of the magnetic-induction waveguide [13]. Ma et al. proposed two-dimensional and three-dimensional regular hexagonal coil arrays and, by optimizing the coupling coefficient, improved the system bandwidth by approximately 15% [14]. Guo and Sun utilized metamaterials to achieve multiband resonance [15]. These methods require large deployment spaces and special fabrication processes. This not only restricts the practicality of the devices in confined or harsh environments but also increases system cost and manufacturing difficulty. Gwynne-Timothy and Bousquet proposed rapidly switching the resonant frequency between two fixed frequencies within a single symbol period to achieve spectrum stretching and bandwidth expansion. However, this method imposes stringent demands on the response speed and stability of the tuning circuit, posing significant implementation challenges [16].

* Corresponding author: Lihua Li (0909031014@nue.edu.cn).

doi:10.2528/PIERL26052102

This study proposes a magnetic induction antenna with a graded-radius structure. Unlike existing bandwidth extension methods, this design achieves a wider continuous frequency band by optimizing the antenna structure, without requiring additional coils or dynamic circuits. The principle is to increase the antenna's resistance to inductance ratio, thereby extending the bandwidth. Simulations and experiments showed that, compared with the uniform-radius structure, the proposed antenna achieved nearly double the bandwidth. However, we confirmed that this extension comes at the expense of reduced coupling strength between coils. Further experimental results indicated that when the bandwidth was extended to nearly twice that of the uniform-radius antenna, the received power at the receiver 1 m away decreased by 6.4 dBm.

2. THEORETICAL ANALYSIS

2.1. Antenna Bandwidth

Because a magnetic induction antenna does not rely on radiation fields, the equivalent series resistance R is usually much smaller than the reference impedance $50\,\Omega$, resulting in a severe port mismatch. Consequently, it is difficult to define bandwidth using conventional VSWR or return-loss metrics. To address this, we introduce an intrinsic 3 dB bandwidth $\Delta f_{3\,\mathrm{dB}}$ as a metric for evaluating the bandwidth of different antenna structures.

The term "3 dB" in $\Delta f_{3\,\mathrm{dB}}$ originates from the halving of power. It refers to the bandwidth over which, in a series resonant circuit, the power P drops from its maximum $P_{\max}$ to $P_{\max}$ as the frequency deviates from resonance. Because $P \propto I^2$, a halving of power is equivalent to the loop current I falling to $\sqrt{2}I/2$, which also means that the impedance magnitude rises from R at resonance to $\sqrt{2}R$.

The impedance magnitude of a series resonant circuit is:

$$|Z| = \sqrt{R^2 + \left(\omega L - \frac{1}{\omega C}\right)^2} \tag{1}$$

Setting $|Z| = \sqrt{2}R$ yields two angular frequencies:

$$\begin{aligned} \omega_1 &= \frac{-R + \sqrt{R^2 + 4L/C}}{2L} \\ \omega_2 &= \frac{R + \sqrt{R^2 + 4L/C}}{2L} \end{aligned} \tag{2}$$

Subtracting the two equations gives:

$$\Delta f_{3\,\mathrm{dB}} = \frac{\Delta\omega}{2\pi} = \frac{R}{2\pi L} \tag{3}$$

It can be seen that $\Delta f_{3\,\mathrm{dB}}$ is proportional to R/L. Therefore, to broaden the bandwidth, it is necessary to increase this ratio, i.e., to reduce the equivalent inductance or increase the equivalent resistance.

2.2. Impedance Analysis of Coils with Different Structures

Equation (3) indicates that the bandwidth of the antenna is directly proportional to the equivalent resistance R and inversely proportional to the equivalent inductance L. Therefore, extending the bandwidth primarily relies on increasing the R/L ratio. To investigate the influence of the gradient-radius structure on the bandwidth, we analyzed how it alters the coil's resistance and inductance.

2.2.1. Inductance Comparison of Different Coil Structures

The total inductance of a multi-turn coil is the sum of the self-inductance of all its turns and the mutual inductance among all pairs of turns [17]:

$$L_{\text{total}} = \sum_{i=1}^{N} L_{s,i} + 2\sum_{i=1}^{N-1}\sum_{j=i+1}^{N} M_{ij} \tag{4}$$

where N is the number of turns; $L_{s,i}$ is the self-inductance of the i-th turn; and M_{ij} is the mutual inductance between the i-th and j-th turns.

The self-inductance of a single-turn circular coil is approximately [18]:

$$L = \mu_0 R\left(\ln\frac{8R}{r} - \frac{7}{4}\right) \tag{5}$$

where μ_0 is the permeability of free space; R is the loop radius; and r is the wire radius. Evidently, the self-inductance is a monotonically increasing function of coil radius.

When comparing the inductance of the traditional structure with that of the proposed gradient-radius structure, the former has a uniform coil radius, and the latter consists of a series of discrete radius values. Figure 1 shows the front and side views of the gradient-radius structure, where the top layer radius is $R_{\min}$, and the bottom layer is $R_{\max}$, and the height is H.

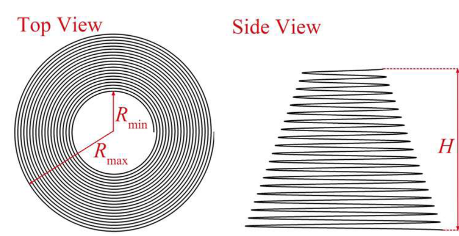

FIGURE 1. Top and side views of the gradient-radius structure.

Assume that both coils have N turns and a pitch of d. The radius of each turn is R_0 for the constant-radius structure, and for the gradient-radius structure, the radius of the i-th turn is R_i, satisfying $R0_{\max}$, with the remaining turns having radii $Ri_{\max_{\min}}$.

From the monotonicity of the self-inductance function, for any turn i, it follows that $L_s(R_i) \le L_s(R_0)$. Therefore, the total self-inductance of the gradient-radius coil is expressed as:

$$\sum_{i=1}^{N} L_s(R_i) \le \sum_{i=1}^{N} L_s(R_0) = N L_s(R_0) \tag{6}$$

The mutual inductance between two coaxial circular rings can be expressed by the first-order approximation of the Neumann formula as follows [19]:

$$M(R_i, R_j, d_{ij}) \approx \frac{\mu_0 \pi R_i R_j}{2\sqrt{\left(\frac{R_i + R_j}{2}\right)^2 + d_{ij}^2}} \tag{7}$$

where d_{ij} is the distance between the two turns, and R_i and R_j are the radii of the two turns. When the inter-turn spacing is determined, the numerator grows faster with the radius than the denominator; therefore, Equation (7) is an increasing function of the coil radii R_i and R_j. For the constant-radius structure, the mutual inductance between any two turns is $M(R_0, R_0, d_{ij})$, whereas for the gradient-radius structure, it is $M(R_i, R_j, d_{ij})$. Since $R_i, R_j \leq R_0$, it follows that:

$$M(R_i, R_j, d_{ij}) \leq M(R_0, R_0, d_{ij}) \tag{8}$$

Therefore, the total mutual inductance of the gradient-radius structure satisfies:

$$\sum_{i<j} M(R_i, R_j, d_{ij}) \leq \sum_{i<j} M(R_0, R_0, d_{ij}) \tag{9}$$

Combining Equations (4), (6), and (9), the following relation is obtained:

$$L_{\text{taper}} = \sum_{i=1}^{N} L_s(R_i) + 2\sum_{i<j} M(R_i, R_j, d_{ij})$$

$$\leq \sum_{i=1}^{N} L_s(R_0) + 2\sum_{i<j} M(R_0, R_0, d_{ij}) = L_{\text{equal}} \tag{10}$$

Here, L_{taper} and L_{equal} represent the total inductance of the gradient-radius and constant-radius coils, respectively. This equation demonstrates that, under identical turn counts and axial arrangements, the total inductance of a gradient-radius coil is lower than that of a constant-radius coil.

2.2.2. Resistance Comparison of Different Coil Structures

While the reduced average radius of the gradient-radius structure shortens the total conductor length and reduces the ohmic resistance determined by the wire material, the equivalent series resistance at high frequencies is dominated by the skin and proximity effects. The latter is particularly significant for tightly wound coils. Although the gradient-radius structure alters the inter-turn magnetic field distribution, it may introduce more complex eddy current paths at the smaller radius end, thus limiting the reduction in the proximity effect resistance. Consequently, the gradient-radius structure achieved only a limited overall reduction in total resistance.

In summary, the gradient-radius structure significantly reduced inductance but only marginally suppressed the resistance, leading to an increased R/L ratio. As indicated by Equation (3), this structural modification effectively extends the bandwidth of the magnetic induction coil.

2.3. Near-Field Magnetic Field Intensity Analysis

According to the Biot-Savart law, the magnetic-field intensity produced by a single-turn coil at a point P on its axis is given by:

$$B = \frac{\mu_0 I}{2} \cdot \frac{R^2}{(R^2 + Z^2)^{3/2}} \tag{11}$$

where I is the coil current; R is the coil radius; and Z is the distance from point P to the coil. Since the communication distance in magnetic induction is typically much larger than the antenna's physical height, Z is treated as a constant in this section.

To investigate the effect of the gradient-radius structure on the magnetic field intensity at point P, let the fractional term involving R in Equation (11) be:

$$f(R) = \frac{R^2}{(R^2 + Z^2)^{3/2}} \tag{12}$$

Differentiating Equation (12) yields:

$$f'(R) = \frac{2RZ^2}{(R^2 + Z^2)^{5/2}} \tag{13}$$

In Equation (13), both R and the denominator are always positive; therefore, the sign of the fraction is determined by $(2Z^2 - R^2)$. When $Z > \sqrt{2}R/2$, we have $f'(R) > 0$, so $f(R)$ is a monotonically increasing function of R. Combined with Equation (11), this indicates that the magnetic-field intensity decreases as the radius R decreases. As a non-radiative near-field communication method, the antenna geometry in magnetic induction communication does not need to be comparable to the wavelength, and the communication distance is much larger than the antenna's physical size; hence, most application scenarios satisfy the above condition.

The magnetic field produced by the magnetic induction antenna at point P is:

$$B_{\text{total}} = \sum_{i=1}^{n} B_i \tag{14}$$

where B_i is the magnetic-field intensity produced individually by the i-th turn at point P, and n is the total number of turns. In the gradient-radius structure, the i-th turn satisfies $R_i < R_{\text{max}}$. Based on the preceding analysis, the produced magnetic-field intensity satisfies $B_i < B_{\text{max}}$. For a uniform structure with all turns having radius R_{max}, the magnetic field intensity of each turn is B_{max}. In summary, from Equation (14), it can be seen that the total near-field magnetic field intensity of the gradient-radius structure is reduced compared with that of the conventional uniform structure.

3. SIMULATION AND EXPERIMENT

3.1. Simulation Results in FEKO

The taper ratio of the gradient-radius coil is defined as:

$$\alpha = 1 - \frac{R_{\text{min}}}{R_{\text{max}}} \tag{15}$$

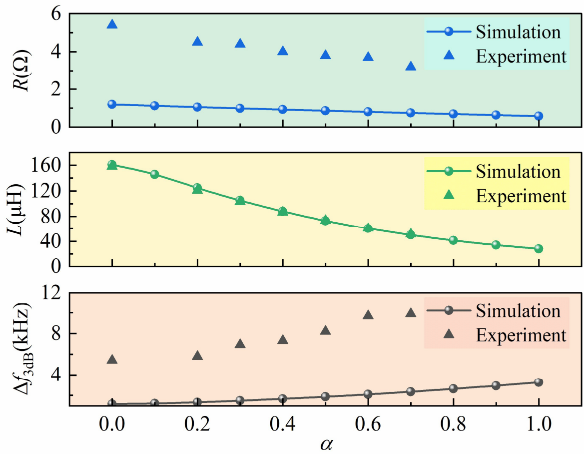

FIGURE 2. Impedance parameters and intrinsic bandwidth of coils with different taper ratios.

R_{min} and R_{max} represent the minimum and maximum radii of the gradient coils, respectively. $\alpha = 0$ represents the conventional uniform-radius coil. In the simulations, R_{max} was 10 cm; the coil height was $H = 2$ cm; and the excitation frequency was 1 MHz. Eleven coils with different taper ratios ranging from 0 to 1 were wound. The resistance and inductance values of the 11 coils were obtained as shown in Figure 2, and the corresponding $\Delta f_{3\,\text{dB}}$ for each coil was calculated according to Equation (3) and plotted in Figure 2.

The simulation results were consistent with the theoretical analysis in Section 2: as the taper ratio increases, the inductance drops significantly while the resistance decreases slightly, thereby extending the intrinsic 3 dB bandwidth $\Delta f_{3\,\text{dB}}$. When α increases from 0 to 1, $\Delta f_{3\,\text{dB}}$ rises from 1.17 kHz to 3.24 kHz, corresponding to a bandwidth gain of more than double.

To further verify the relationship between bandwidth enhancement and magnetic field attenuation in the gradient-radius structure, two magnetic induction coils were established in the simulation software. One coil served as the transmitting antenna, whose taper ratio was also increased from 0 to 1, and the other served as the receiving antenna with a fixed taper ratio of 0. The communication distance was 0.2 m, and S_{21} parameters

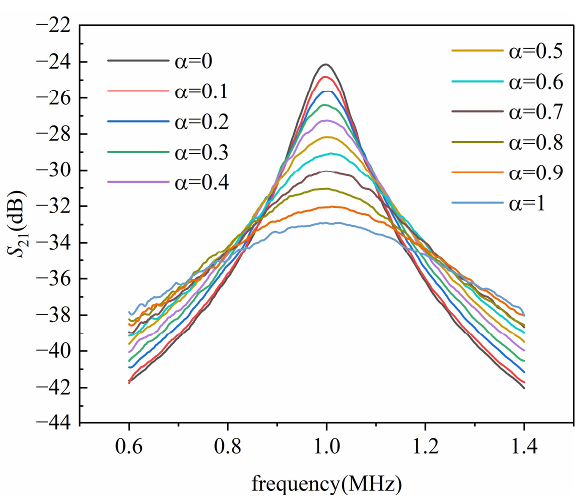

FIGURE 3. S_{21} curves of coils with different taper ratios.

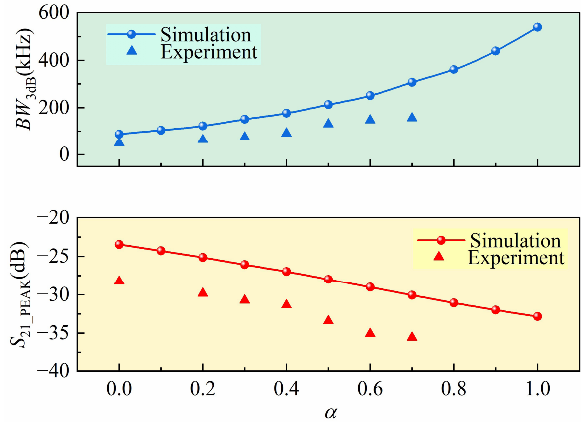

FIGURE 4. S_{21} peak value and bandwidth of coils with different taper ratios.

of the coils with different taper ratios were measured over the frequency band from 0.6 to 1.4 MHz and plotted in Figure 3. The curves in Figure 4 show the peak value of S_{21} denoted as S_{21_PEAK} and the 3 dB bandwidth $BW_{3\,\text{dB}}$ as functions of α. It can be observed that as α increased, the S_{21} curves became wider; S_{21_PEAK} decreased; and $BW_{3\,\text{dB}}$ increased. The 3 dB bandwidth shown in Figure 4 is the bandwidth in the magnetic induction communication system, not the antenna's intrinsic bandwidth.

3.2. Experimental Verification

Because achieving a taper ratio of 1 is challenging in practice, we only fabricated physical antennas with taper ratios of 0 and from 0.2 to 0.7, as shown in Figure 5. To minimize errors caused by manufacturing tolerances, three replicates of each design were produced. All subsequent experimental data were averaged over these three measurements. The antenna framework utilized polylactic acid, a material characterized by a material with magnetic permeability similar to vacuum and ultralow electrical conductivity (approximately 10^{-10} S/m). This ensured that the framework did not interfere with the coil-generated magnetic field. However, its relative permittivity was about 2, resulting in non-negligible dielectric losses.

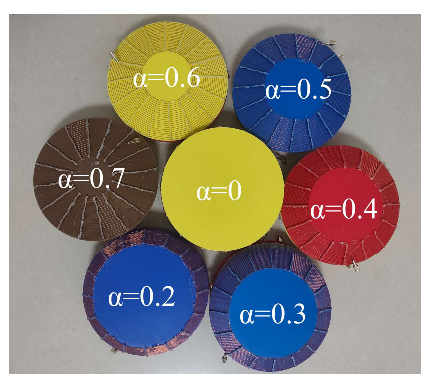

FIGURE 5. Physical antennas with different taper ratios.

The impedance analyzer shown in Figure 6 was used to measure the inductance and resistance of the antennas with different

FIGURE 6. Impedance measurement experiment.

TABLE 1. Impedance of physical coils with different taper ratios.

α	R (Ω)	L (μH)
0	3.2	51.4
0.2	3.7	60.7
0.3	3.8	73.6
0.4	4.0	86.9
0.5	4.5	103.3
0.6	4.4	120.9
0.7	5.4	158.3

taper ratios. The results were recorded in Table 1 and plotted in Figure 2 as scatter points.

The measured inductance was close to the simulated values, but the resistance was higher. This was because the simulation modeled only the coil itself, while the physical prototype contained a polylactic acid frame. This material introduces additional dielectric loss under an alternating electric field, leading to an increase in the measured resistance. Since the measured resistance was larger, the intrinsic bandwidth calculated from Equation (3) was broader than the simulated result.

To evaluate bandwidth gain and energy loss, we measured antennas' S_{21} parameters with different taper ratios at a communication distance of 20 cm. The experimental setup is shown in Figure 7. The transmitting antenna, after being tuned, was linked to Port 1 of the vector network analyzer, while the receiving antenna was linked to Port 2. The measured S_{21} curves for different taper ratios are shown in Figure 8.

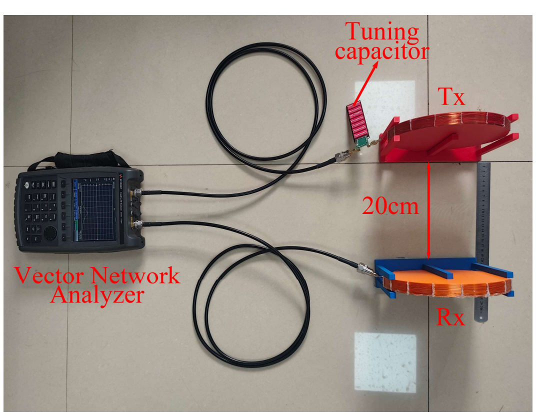

FIGURE 7. S_{21} test scenario.

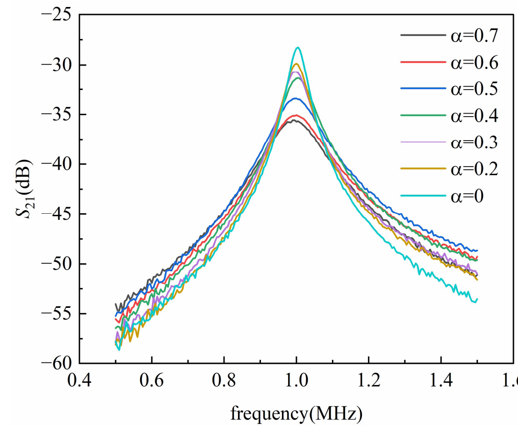

FIGURE 8. Measured S_{21} curves.

Figures 8 and 3 show similar patterns. As the taper ratio α increases, the S_{21} curves become wider and lower, resulting in a decrease in the S_{21} peak and an increase in the bandwidth. Similarly, S_{21_PEAK} and $BW_{3\,\mathrm{dB}}$ were extracted from the measured S_{21} curves and plotted as scatter points in Figure 4.

The measured $BW_{3\,\mathrm{dB}}$ was nearly half of the simulated value, and the measured S_{21_PEAK} was lower than the simulated values. It attributed to the additional losses introduced by the tuning capacitors and the solder joints of the SMA connectors.

To further verify that increasing the taper ratio leads to reducing the coupling strength, experiments were conducted at a communication distance of 1 m using a signal generator as the source and monitoring the received power with a spectrum analyzer. The experimental setup is shown in Figure 9.

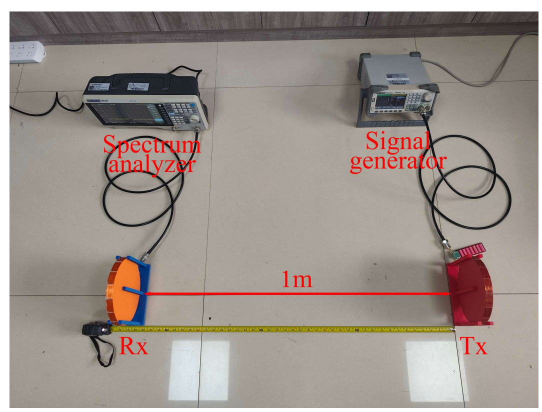

FIGURE 9. Communication test scenario.

The signal generator was set to output a sinusoidal wave with an amplitude of 1 Vpp at a frequency of 1 MHz. Meanwhile, a spectrum analyzer was used at the receiving end to measure the power, and the results were recorded in Table 2. As α increases from 0 to 0.7, the received power decreases by 6.4 dBm, meaning that the received power at $\alpha = 0.7$ is only one-fifth of that at $\alpha = 0$. In summary, the taper ratio involves a trade-off between bandwidth gain and magnetic field attenuation, which must be considered to design a gradient-radius magnetic induction antenna that meets the communication requirements.

TABLE 2. Effect of taper ratio structure on received power.

α	Rx power (dBm)
0	69.5
0.2	68.7
0.3	67.5
0.4	66.3
0.5	65.6
0.6	64.5
0.7	63.1

4. CONCLUSION

In this study, a magnetic induction antenna with a gradient-radius structure was proposed to extend bandwidth by increasing the resistance-to-inductance ratio. Experimental results demonstrated that bandwidth gains scale with the taper ratio. Both simulations and measurements showed that at 1 MHz, a coil with a taper ratio of 0.7 extended the bandwidth to nearly twice that of the uniform-radius counterpart. However, the reduced coil radius leads to weaker generated magnetic fields. Experimental data indicated that at a 20 cm distance, the tapered coil yielded roughly double bandwidth at the expense of a 6.4 dBm drop in received power. Therefore, practical designs should avoid maximizing bandwidth alone; instead, a careful trade-off between bandwidth and coupling strength is required.

ACKNOWLEDGEMENT

This work was supported in part by the Self-developed scientific research project of Naval University of Engineering (2025236).

REFERENCES

[1] Sun, Z. and I. F. Akyildiz, "Magnetic induction communications for wireless underground sensor networks," *IEEE Transactions on Antennas and Propagation*, Vol. 58, No. 7, 2426–2435, 2010.

[2] Kim, J.-Y., H. J. Lee, J. H. Oh, K.-S. Yoon, and I.-K. Cho, "Magnetic induction-based test-bed system for magnetic communication in underground mines," in *2023 20th Annual IEEE International Conference on Sensing, Communication, and Networking (SECON)*, 388–389, Madrid, Spain, 2023.

[3] Bamhdi, A. M., "Underwater magnetic induction communication range enhancement survey and comprehensive evaluation," *International Journal of Advances in Soft Computing and its Applications*, Vol. 16, No. 2, 207–230, 2024.

[4] Malik, P. S., M. Abouhawwash, A. Almutairi, R. P. Singh, and Y. Singh, "Comparative analysis of magnetic induction based communication techniques for wireless underground sensor networks," *PeerJ Computer Science*, 2022.

[5] Yoon, K.-S., J. H. Oh, H. J. Lee, J.-Y. Kim, and I.-K. Cho, "Wideband magnetic induction wireless communications in challenging underground environments: A current-driven scheme," *IEEE Internet of Things Journal*, Vol. 12, No. 13, 24 929–24 943, 2025.

[6] Liu, B. H., Y. B. Wang, and T. H. Fu, "Research on the model and characteristics of underground magnetic induction communication channel," *Progress In Electromagnetics Research M*, Vol. 101, 89–100, 2021.

[7] Cannon, B. L., J. F. Hoburg, D. D. Stancil, and S. C. Goldstein, "Magnetic resonant coupling as a potential means for wireless power transfer to multiple small receivers," *IEEE Transactions on Power Electronics*, Vol. 24, No. 7, 1819–1825, 2009.

[8] Doan Thanh, H., "Ofdm in near field magnetic induction communication," Ph.D. dissertation, La Trobe University, Melbourne, Victoria, Australia, 2016.

[9] Dionigi, M. and M. Mongiardo, "A novel resonator for simultaneous wireless power tranfer and near field magnetic communications," in *2012 IEEE/MTT-S International Microwave Symposium Digest*, 1–3, Montreal, QC, Canada, 2012.

[10] Agbinya, J. I. and H. Nguyen, "Principles and applications of frequency splitting in inductive communications and wireless power transfer systems," *Wireless Personal Communications*, Vol. 107, No. 2, 987–1017, 2019.

[11] Oh, T., I.-K. Cho, H. J. Lee, and J.-Y. Kim, "Design of multi-resonant loop antenna for magnetic induction communication," in *2022 13th International Conference on Information and Communication Technology Convergence (ICTC)*, 2086–2088, Jeju Island, Korea, Republic of, 2022.

[12] Sun, Z., I. F. Akyildiz, S. Kisseleff, and W. Gerstacker, "Increasing the capacity of magnetic induction communications in RF-challenged environments," *IEEE Transactions on Communications*, Vol. 61, No. 9, 3943–3952, 2013.

[13] Syms, R. R. A., L. Solymar, I. R. Young, and T. Floume, "Thin-film magneto-inductive cables," *Journal of Physics D: Applied Physics*, Vol. 43, No. 5, 055102, 2010.

[14] Ma, J., X. Zhang, M. Liao, and J. He, "Topology of magneto-inductive communication system based on the regular hexagonal array," *IET Microwaves, Antennas & Propagation*, Vol. 9, No. 5, 389–398, 2015.

[15] Guo, H. and Z. Sun, "Increasing the capacity of magnetic induction communication using MIMO coil-array," in *2016 IEEE Global Communications Conference (GLOBECOM)*, 1–6, Washington, DC, USA, 2016.

[16] Gwynne-Timothy, T. and J.-F. Bousquet, "Wireless transmitter bandwidth extension using dynamically varying capacitors," in *2015 IEEE 28th Canadian Conference on Electrical and Computer Engineering (CCECE)*, 202–207, Halifax, NS, Canada, 2015.

[17] Rosa, E. B. and F. W. Grover, *Formulas and Tables for the Calculation of Mutual and Self-inductance*, US Government Printing Office, 1912.

[18] Ren, Y., G. Kuang, and W. Chen, "Inductance of bitter coil with rectangular cross-section," *Journal of Superconductivity and Novel Magnetism*, Vol. 26, No. 6, 2159–2163, 2013.

[19] Grover, F. W., *Inductance Calculations: Working Formulas and Tables*, Courier Corporation, 2004.